

Inelastic vector soliton collisions: a lattice-based quantum representation

BY GEORGE VAHALA¹, LINDA VAHALA² AND JEFFREY YEPEZ³

¹*Department of Physics, College of William and Mary, Williamsburg, VA 23187-8795, USA (vahala@niv.physics.wm.edu)*

²*Department of Electrical and Computer Engineering, Old Dominion University, Norfolk, VA 23529, USA*

³*Air Force Research Laboratory, Hanscom AFB, MA 01731-3010, USA*

Published online 3 June 2004

Lattice-based quantum algorithms are developed for vector soliton collisions in the completely integrable Manakov equations, a system of coupled nonlinear Schrödinger (coupled-NLS) equations that describe the propagation of pulses in a birefringent fibre of unity cross-phase modulation factor. Under appropriate conditions the exact 2-soliton vector solutions yield inelastic soliton collisions, in agreement with the theoretical predictions of Radhakrishnan *et al.* (1997 *Phys. Rev. E* **56**, 2213). For linearly birefringent fibres, quasi-elastic solitary-wave collisions are obtained with emission of radiation. In a coupled integrable turbulent NLS system, soliton turbulence is found with mode intensity spectrum scaling as k^{-6} .

Keywords: vector solitons; Manakov equations; inelastic soliton collisions; quantum lattice gas algorithms; turbulence

1. Introduction

There is much to be gained in using micro or meso descriptions for macroscopic processes. For example, the straightforward solution of the nonlinear conservation equations (e.g. the Navier–Stokes equation for fluid turbulence) is faced with the problem of determining an accurate resolution of nonlinear convective derivatives. This so-called Riemann problem is computationally very expensive (Peyret 1996). However, if one proceeds to a mesoscopic description using the lattice Boltzmann equation with the linearized BGK collision operator (Succi 2001), then one finishes with a simple highly parallelized algorithm which in the long-wavelength long-time limit recovers the original nonlinear macroscopic equations. The nonlinear convective derivatives of the macroscopic system are replaced by simple linear (kinetic) advection in the mesoscopic lattice Boltzmann scheme. Alternatively, one could consider a microscopic representation such as a lattice gas model with its detailed kinetic two-body and three-body lattice collision rules (Frisch *et al.* 1987).

The nonlinear Schrödinger (NLS) equation has played a pivotal role in soliton physics and, in particular, optical solitons (Kivshar & Agrawal 2003). Here we

One contribution of 21 to a Theme ‘Connecting scales: micro, meso and macro processes’.

develop at the microscopic scales a quantum lattice gas (QLG) algorithm to examine vector solitons in certain classes of NLS equations. The impetus behind quantum algorithms lies in their exponential speed-up over classical algorithms (as, for example, illustrated by the Shor (1994) quantum factoring algorithm over classical factoring schemes). The fundamental change in moving from a classical to quantum algorithm is to replace the classical binary bits ‘0’ and ‘1’ by the quantum states $|0\rangle$ and $|1\rangle$. It is the entanglement of multiple qubits, a purely quantum property that has no counterpart in classical physics, that can lead to exponential speed-up (Nielsen & Chuang 2000). In the quantum algorithms presented here, this qubit entanglement is achieved by a unitary collision operator coupling on-site qubits. This entanglement is then spread throughout the lattice by unitary streaming operators. Quantum coherence needs to be retained during the application of a sequence of these collide-stream unitary operators, until quantum measurement is required to determine the amplitude of the wave function.

Soliton transmission in optical fibres is an important aspect of long-distance (transoceanic) communication. However, optical fibres are birefringent, and a single-mode fibre can support two distinct orthogonal polarizations: the O-mode, which has a constant refractive index along the ray path, and the X-mode, whose refractive index varies along the ray path. Hence pulses with components in these orthogonal polarizations will travel at slightly different speeds. It can be shown (Lakshmanan & Kanna 2001) that the slowly varying amplitudes of these modes satisfy the coupled-NLS equations

$$\left. \begin{aligned} i\frac{\partial Q_1}{\partial t} + \frac{\partial^2 Q_1}{\partial x^2} + 2\mu[|Q_1|^2 + B|Q_2|^2] \cdot Q_1 &= 0, \\ i\frac{\partial Q_2}{\partial t} + \frac{\partial^2 Q_2}{\partial x^2} + 2\mu[|Q_2|^2 + B|Q_1|^2] \cdot Q_2 &= 0, \end{aligned} \right\} \quad (1.1)$$

where μ is a positive coefficient,

$$B = \frac{2 + 2\sin^2\theta}{2 + \cos^2\theta}$$

is the cross-phase modulation coefficient and θ is the birefringence ellipticity angle (Menyuk 1989). In general, the coupled-NLS system equation (1.1) is non-integrable. However, for the special case $B = 1$, equation (1.1) is completely integrable and is known as the Manakov (1974) system. The Manakov equations also describe the effects of mean random birefringence on the propagation of a circularly polarized pulse down a real fibre.

In § 2, we shall briefly review the exact analytic solutions for 1-soliton and 2-solitons in the scalar and vector NLS equations. While the scalar NLS soliton-collision properties are well known—the solitons retain their exact shape and speed after the collision and suffer only a small spatial shift as the signature that a collision has occurred—it has only recently been discovered (Radhakrishnan *et al.* 1997) that vector 2-soliton collisions for the fully integrable Manakov system (equation (1.1) with $B = 1$) can suffer *inelastic* collisions. This has led to a flurry of activity (Jakubowski *et al.* 1998; Steiglitz 2001*a, b*) in designing sequences of such soliton collisions that can affect logic operations (e.g. controlled-NOT gates) and so manipulate solitons to perform computations. In § 3, we present the QLG representation for the coupled-NLS system.

However, the algorithm is sufficiently general that it can handle arbitrary nonlinear potential interactions, not just the cubic nonlinearity of the Manakov system. We find that we require two qubits per scalar field at each lattice node. The one-particle sector representation of the Hilbert space allows us to restrict the dimensionality of the wave-function probability amplitudes to just the dimensionality of the number of on-site qubits. In § 4 we present the simulation results of the QLG representation for the completely integrable Manakov system ($B = 1$) as well as for the quasi-integrable solitary-wave solutions to the coupled-NLS equations with $B = 0.667$ (this corresponds to a pulse propagating down a linear birefringent fibre). Turbulent soliton interactions are also considered using a potential of the form $\sqrt{2\mu[|Q_1|^2 + |Q_2|^2]}$ in the evolution of the Q_2 -mode, while the Q_1 -mode satisfies the standard cubic NLS potential. We have presented some preliminary results on the *elastic* Manakov soliton collisions at a SPIE conference (Vahala *et al.* 2003a). Here, we concentrate on those soliton parameters that permit *inelastic* Manakov soliton collisions, and consider the effect of the cross-phase modulation coefficient and turbulence on the soliton/solitary waves. (We restrict our use of the word ‘soliton’ to strictly mean a form-invariant propagating pulse following nonlinear collisions.) Finally, in § 5 we present our summary and conclusions.

2. Inelastic soliton collisions

(a) Exact 2-soliton solutions

Consider the completely integrable Manakov system, equation (1.1), with cross-phase modulation coefficient $B = 1$. The 1-soliton vector solution (2.4) has components

$$Q_1(x, t) = \begin{cases} \frac{1}{2}\alpha \exp[-\frac{1}{2}R + i\eta_I] \operatorname{sech}[\eta_R + \frac{1}{2}R], \\ \frac{1}{2}\beta \exp[-\frac{1}{2}R + i\eta_I] \operatorname{sech}[\eta_R + \frac{1}{2}R], \end{cases} \quad (2.1)$$

with complex

$$\eta = \eta_R + i\eta_I = k(x + ikt). \quad (2.2)$$

The parameter R is real:

$$R = \ln \left[\frac{\mu(|\alpha|^2 + |\beta|^2)}{4k_R^2} \right], \quad (2.3)$$

while α , β and k are arbitrary complex parameters with $k_R \neq 0$. k_I determines the velocity of the 1-soliton components.

Using the Hirota method, Radhakrishnan *et al.* (1997) have generated exact 2-soliton vector solutions to the Manakov system, valid for all time. These solutions are quite complicated. However, of specific interest here are the asymptotic limits in which these 2-soliton solutions reduce to a sum of two widely separated (non-overlapping) 1-soliton solutions

$$\left. \begin{aligned} Q_1(x, t) &= \sum_{n=1}^2 \frac{1}{2}\alpha_n \exp[-\frac{1}{2}R_n + i\eta_{nI}] \operatorname{sech}[\eta_{nR} + \frac{1}{2}R_n], \\ Q_2(x, t) &= \sum_{n=1}^2 \frac{1}{2}\beta_n \exp[-\frac{1}{2}R_n + i\eta_{nI}] \operatorname{sech}[\eta_{nR} + \frac{1}{2}R_n], \end{aligned} \right\} \quad (2.4)$$

$$\eta_n = \eta_{nR} + i\eta_{nI} = k_n(x - x_{0n} + ik_n t), \quad R_n = \ln \left[\frac{\mu(|\alpha_n|^2 + |\beta_n|^2)}{4k_{nR}^2} \right], \quad (2.5)$$

with appropriately chosen free complex parameters α_n , β_n and k_n , $n = 1, 2$. The (real) parameters x_{0n} predominantly determine the spatial position of the peaks of the two widely separated 1-solitons, k_{nR} the 1-soliton amplitudes and k_{nI} the 1-soliton velocities.

(b) *Asymptotic post-collision solitons*

The *post-collision* 2-soliton vector solution will also asymptotically reduce to two non-overlapping vector 1-solitons of the form of equations (2.4) and (2.5). In particular, for the choice $k_{1R} > 0$, $k_{2R} > 0$, the post-collision non-overlapping 1-soliton amplitude ratios are given by (2.5)

$$\left. \begin{aligned} \frac{\alpha'_1}{\beta'_1} &= \left(\left[1 - g + \left| \frac{\alpha_1}{\beta_1} \right|^2 \right] \frac{\alpha_2}{\beta_2} + g \frac{\alpha_1}{\beta_1} \right) \left(g \frac{\alpha_1^*}{\beta_1^*} \frac{\alpha_2}{\beta_2} + (1 - g) \left| \frac{\alpha_1}{\beta_1} \right|^2 + 1 \right)^{-1}, \\ \frac{\alpha'_2}{\beta'_2} &= \left(\left[1 - h^* + \left| \frac{\alpha_2}{\beta_2} \right|^2 \right] \frac{\alpha_1}{\beta_1} + h^* \frac{\alpha_2}{\beta_2} \right) \left(h^* \frac{\alpha_2^*}{\beta_2^*} \frac{\alpha_1}{\beta_1} + (1 - h^*) \left| \frac{\alpha_2}{\beta_2} \right|^2 + 1 \right)^{-1}, \end{aligned} \right\} \quad (2.6)$$

where

$$g(k_1, k_2) = \frac{2k_{1R}}{k_2 + k_1^*}, \quad h(k_1, k_2) = \frac{2k_{2R}}{k_1 + k_2^*} \quad (2.7)$$

Note that the k_n are invariant under soliton collisions. It is clear that a certain choice of these complex k_n will result in elastic 2-soliton vector collisions, as is always found in scalar soliton collisions, but most choices of k_n will result in inelastic 2-soliton vector collisions. In particular, there is a choice of parameters for the k_n such that

$$a'_i = 0, \quad (2.8)$$

i.e. for the polarization mode Q_1 , its initial non-overlapping 2-solitons will in its post-collision state have only a single outgoing soliton. It is this type of inelastic soliton collision that has encouraged research into an all-soliton digital information processor in a nonlinear optical media without radiative losses (Jakubowski *et al.* 1998; Steiglitz 2001a, b).

3. Quantum lattice gas representation for coupled-NLS

Here we generalize our QLG algorithm for the scalar NLS equation (Vahala *et al.* 2003a) to the coupled vector NLS system for arbitrary coupling potentials V_1 and V_2 ,

$$\left. \begin{aligned} i \frac{\partial Q_1}{\partial t} + \frac{\partial^2 Q_1}{\partial x^2} + V_1[|Q_1|, |Q_2|] \cdot Q_1 &= 0, \\ i \frac{\partial Q_2}{\partial t} + \frac{\partial^2 Q_2}{\partial x^2} + V_2[|Q_2|, |Q_1|] \cdot Q_2 &= 0. \end{aligned} \right\} \quad (3.1)$$

Our NLS formulation was based on the one particle sector representation introduced by Yezep & Boghosian (2002) in their quantum algorithm for the (linear) Schrödinger equation. The spatial domain is discretized into L spatial nodes and two qubits per

scalar wave function are introduced at each node x_ℓ , $\ell = 1, \dots, L$, i.e. qubits $|q_{0,1}^\ell\rangle$ for the scalar field Q_1 and qubits $|q_{2,3}^\ell\rangle$ for Q_2 at x_ℓ . A unitary collision operator that will recover equation (3.1) is a factored collision operator that only entangles on-site qubits, and actually only the on-site qubits, pairwise, corresponding to that particular scalar field. The on-site coupling of all the four qubits $|q_i^\ell\rangle$, $i = 1, \dots, 4$ is attained by introducing a phase transformation of the wave functions.

In the number representation of the 1-particle sector, the basis set factors into

$$|n_0^1 n_1^1 \dots n_0^L n_1^L\rangle |n_2^1 n_3^1 \dots n_2^L n_3^L\rangle, \tag{3.2}$$

where only one of $n_{0,1}^\ell$ is non-zero and equals unity, and similarly for $n_{2,3}^\ell$. Because of the factorization (see equation (3.2)), we need to consider the application of the collision and streaming operators on each qubit pair separately.

(a) Unitary collision operator for the qubit pair $|q_{0,1}\rangle$

To evolve the wave function for the two qubits $|q_{0,1}\rangle$, a global quantum unitary operator \hat{C} is constructed from a tensor product of quantum gates, each independently applied to each spatial site

$$\hat{C} = \bigotimes_{\ell=1}^L \hat{U}_\ell. \tag{3.3}$$

\hat{U}_ℓ locally entangles the two qubits $|q_{0,1}\rangle$ at each site and a local equilibrium can be associated with this on-site unitary collision operator if $|\nu\rangle$ is an eigenvector of \hat{U}_ℓ with unit eigenvalue: $\hat{U}_\ell|\nu\rangle = |\nu\rangle$.

The Schrödinger part of the NLS equation is recovered by the $\sqrt{\text{SWAP}}$ gate $\hat{U}_\ell = \hat{U}$ on a site-by-site basis (2.7)

$$\hat{U}_{\text{NLS}} = \begin{pmatrix} 1 & 0 & 0 & 0 \\ 0 & \frac{1}{2}(1-i) & \frac{1}{2}(1+i) & 0 \\ 0 & \frac{1}{2}(1+i) & \frac{1}{2}(1-i) & 0 \\ 0 & 0 & 0 & 1 \end{pmatrix}. \tag{3.4}$$

with the Hamiltonian representation

$$\hat{U}_{\text{NLS}} = \exp[\frac{1}{8}i\pi] \exp[-\frac{1}{8}i\pi(\sigma_x^1 \sigma_x^2 + \sigma_y^1 \sigma_y^2 + \sigma_z^1 \sigma_z^2)] \tag{3.5}$$

written in terms of the tensor products of the Pauli spin matrices

$$\sigma_x = \begin{pmatrix} 0 & 1 \\ 1 & 0 \end{pmatrix}, \quad \sigma_y = \begin{pmatrix} 0 & -i \\ i & 0 \end{pmatrix}, \quad \sigma_z = \begin{pmatrix} 1 & 0 \\ 0 & -1 \end{pmatrix}$$

for qubits ‘0’ and ‘1’. Note that $\hat{U}_{\text{NLS}}^4 = I$, the identity operator, so $\hat{U}_{\text{NLS}}^4|\nu\rangle = |\nu\rangle$.

(b) Unitary streaming operator for the qubit pair $|q_{0,1}\rangle$

The next step of the QLG algorithm is to stream the post-collision on-site ket for qubits $|q_{0,1}\rangle$ to nearest-neighbour sites. The (unitary) streaming operator \hat{S}_1 is defined as a global shift to the right of qubit $|q_0\rangle$ on each lattice node, i.e.

$$\hat{S}_1 = \prod_{\ell=1}^L \hat{\chi}_{0\ell \rightarrow 0\ell+1}, \tag{3.6}$$

where $\hat{\chi}_{0\ell \rightarrow 0\ell+1}$ is independent of ℓ . The qubit $|q_1\rangle$ is not streamed by \hat{S}_1 . Thus, for the two-qubit pair $|q_{0,1}\rangle$, \hat{U} entangles the on-site qubit pair, while $\hat{\chi}$ operates on the first qubit of neighbouring sites. Hence, the total collision matrix, \hat{C} , does not commute with the full streaming operator \hat{S}_1 .

To symmetrize the algorithm, we also introduce the streaming operator \hat{S}_2 , which performs a global shift to the right of the second qubit on all the lattice nodes for the qubit pair $|q_{0,1}\rangle$:

$$\hat{S}_2 = \prod_{\ell=1}^L \hat{\chi}_{1\ell,1\ell+1}. \quad (3.7)$$

(c) *Introduction of the potential field for the evolution of the wave function for qubit pair $|q_{0,1}\rangle$*

It is known (Bialynicki-Birula 1994; Yepez & Boghosian 2002) that the effect of an external potential $V_1(x)$ can be modelled by the introduction of a local phase change to the system wave function for the qubit pair $|q_{0,1}\rangle$. Let Q_1 denote the wave function for the qubit pair $|q_{0,1}\rangle$. Thus,

$$Q_1(x, t) \rightarrow \exp[iV_1(x)\Delta t]Q_1(x, t), \quad (3.8)$$

where Δt is the time advancement after each step of the algorithm.

We proceed similarly with the qubit pair $|q_{2,3}\rangle$, introducing the $\sqrt{\text{SWAP}}$ gate that entangles the qubits $|q_{2,3}\rangle$ and the streaming operator \hat{S}_1 that shifts qubit $|q_2\rangle$ and \hat{S}_2 that shifts qubit $|q_3\rangle$. One can now introduce another external potential $V_2(x)$ by a local phase change in the system wave function Q_2 for the qubit pair $|q_{2,3}\rangle$:

$$Q_2(x, t) \rightarrow \exp[iV_2(x)\Delta t]Q_2(x, t). \quad (3.9)$$

(d) *Quantum algorithm for coupled-NLS equations*

The collide-stream sequence of unitary operators is applied simultaneously to the qubit pairs $|q_{0,1}\rangle$ and $|q_{2,3}\rangle$:

$$\begin{pmatrix} Q_1(t + \Delta t) \\ Q_2(t + \Delta t) \end{pmatrix} = \begin{pmatrix} [\hat{S}_2^T \hat{C} & \hat{S}_2 \hat{C} & \hat{S}_2^T \hat{C} & \hat{S}_2 \hat{C} \cdot \hat{S}_1^T \hat{C} & \hat{S}_1 \hat{C} & \hat{S}_1^T \hat{C} & \hat{S}_1 \hat{C}] Q_1(t) \\ [\hat{S}_4^T \hat{C} & \hat{S}_4 \hat{C} & \hat{S}_4^T \hat{C} & \hat{S}_4 \hat{C} \cdot \hat{S}_3^T \hat{C} & \hat{S}_3 \hat{C} & \hat{S}_3^T \hat{C} & \hat{S}_3 \hat{C}] Q_2(t) \end{pmatrix}, \quad (3.10)$$

where \hat{S}_i^T is the transpose of \hat{S}_i , with $\hat{S}_i^T \hat{S}_i = I$, $i = 1, 4$ and \hat{C} is the tensor product of the unitary collision operator \hat{U}_{NLS} , equation (3.5). After performing the collide-stream sequence (equation (3.10)), one then introduces the phase change transformations (3.8), (3.9):

$$\begin{pmatrix} Q_1 \\ Q_2 \end{pmatrix} \rightarrow \begin{pmatrix} \exp[V_1(|Q_1|, |Q_2|)\Delta t] \cdot Q_1 \\ \exp[V_2(|Q_1|, |Q_2|)\Delta t] \cdot Q_2 \end{pmatrix}, \quad (3.11)$$

where the potential fields are required to be functions of the wave functions themselves, $V_i = V_i(|Q_1|, |Q_2|)$.

The continuum limit is defined by scaling the spatial shift between neighbouring nodes to be $O(\varepsilon)$, the time advancement $\Delta t = O(\varepsilon^2)$ and the potentials

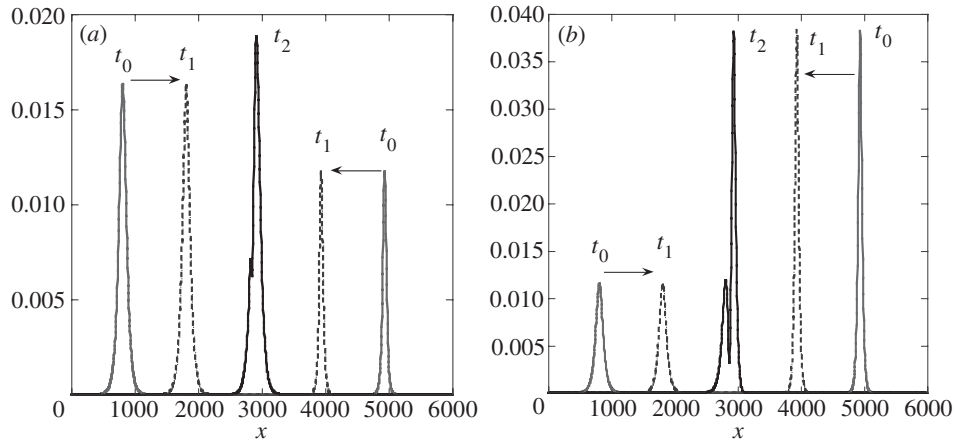


Figure 1. The propagation of an initial ($t_0 = 0$) exact 2-soliton vector solution to the fully integrable Manakov system ($B = 1$) for the polarization modes (a) $|Q_1|$, (b) $|Q_2|$. The solitons propagate towards each other ($t_1 = 25$ K) and undergo their first collision at $t_2 = 50$ K.

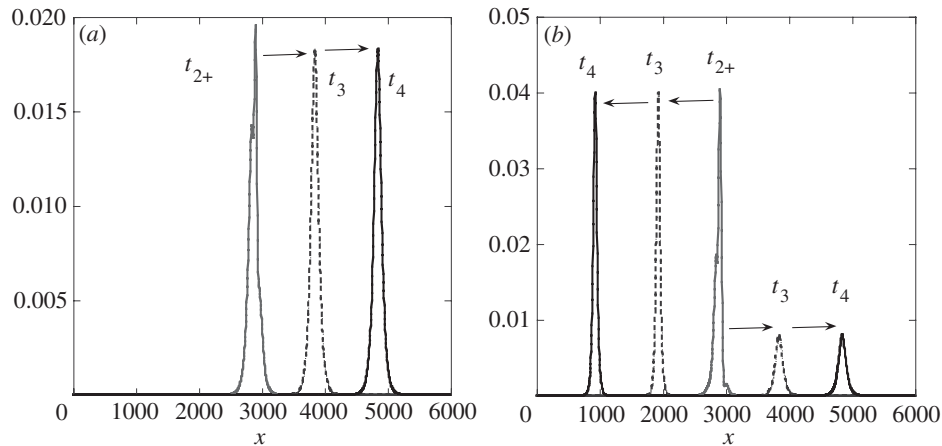


Figure 2. The post-collision polarization modes for soliton parameters, chosen so that there is no left-propagating soliton for mode Q_1 (see equation (2.8)). $t_{2+} = 51$ K, $t_3 = 75$ K and $t_4 = 100$ K. The intensity in each mode $\int dx |Q_i(x, t)|^2 = \text{const.}$ is preserved to better than one part in 10^{-7} . Within each mode, there is redistribution of the intensity in the outgoing asymptotic 1-soliton states.

$V_i = \varepsilon^2 V_i[|Q_1|, |Q_2|]$. In the limit $\varepsilon \rightarrow 0$, it can be shown using MATHEMATICA that the equation (3.10), (3.11) sequence yields the coupled-NLS equations

$$\left. \begin{aligned} i \frac{\partial Q_1}{\partial t} + \frac{\partial^2 Q_1}{\partial x^2} + V_1[|Q_1|, |Q_2|] \cdot Q_1 &= 0 + O(\varepsilon^2), \\ i \frac{\partial Q_2}{\partial t} + \frac{\partial^2 Q_2}{\partial x^2} + V_2[|Q_2|, |Q_1|] \cdot Q_2 &= 0 + O(\varepsilon^2), \end{aligned} \right\} \text{ as } \varepsilon \rightarrow 0, \quad (3.12)$$

with error of $O(\varepsilon^2)$. Equations (3.12) hold for any choice of potentials V_1 and V_2 .

It is also clear how to extend this analysis to a system of N -coupled-NLS equations. N -coupled NLS equations arise in the study of beam propagation in a Kerr-like

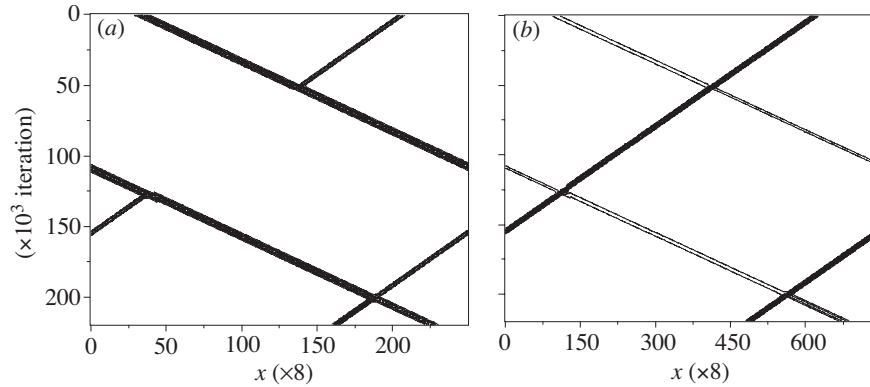


Figure 3. The $x-t$ plot of the 2-soliton vector solution to the Manakov equations under periodic boundary conditions and with the same parameters as for the solutions shown in figures 1 and 2. Soliton–soliton collisions occur around $t = 50$ K, 125 K and 200 K iterations. There is a totally inelastic soliton state for the Q_1 -mode following the first collision. Following the second collision, the outgoing state for Q_1 once again has two solitons.

photorefractive medium, which typically exhibits very strong nonlinear effects with extremely low optical powers. Partially coherent solitons have been observed through excitation by partially coherent light (Mitchell *et al.* 1997) as well as by an ordinary incandescent light bulb (Mitchell & Segev 1997).

It should also be noted that using the 1-particle sector allows the dimensionality of the unitary collision matrix to scale linearly with the number of locally entangled qubits, rather than scale exponentially with the total number of on-site qubits.

4. Quantum lattice gas simulation results on inelastic soliton collisions

(a) Inelastic Manakov vector soliton collisions

For convenience, we consider periodic boundary conditions on a spatial lattice of 6000 nodes for the integrable Manakov equations with cross-phase modulation coefficient $B = 1$. The simulation parameters are chosen so that the 2-vector solitons for the polarization modes Q_1 and Q_2 are initially non-overlapping single solitons, slightly displaced from $x = 1000$ and $x = 5000$, respectively, and moving towards each other for a collisional interaction (at $t_0 = 0$ in figure 1). Moreover, the parameters are chosen so that the theoretical results of equations (2.6)–(2.8) yield the loss of one of these solitons in the Q_1 -mode in the post-collision state.

In figures 1 and 2 we show the results of the QLG algorithm, and indeed find the totally inelastic post-collision state in which the second soliton in mode Q_1 is absent. Moreover, in the fully integrable Manakov system, the total intensity in *each* propagation mode Q_i is conserved, while its distribution among the individual solitons in that mode can be redistributed by soliton collision (see equations (2.6), (2.7)). Our algorithm conserves this total individual mode intensity to better than one part in 10^7 , even in the single-soliton post-collision state. With periodic boundaries, there will be further soliton–soliton collisions, as seen in the $x-t$ plot in figure 3. Between the first and second soliton–soliton collision ($52 \text{ K} < t < 125 \text{ K}$), there is a totally

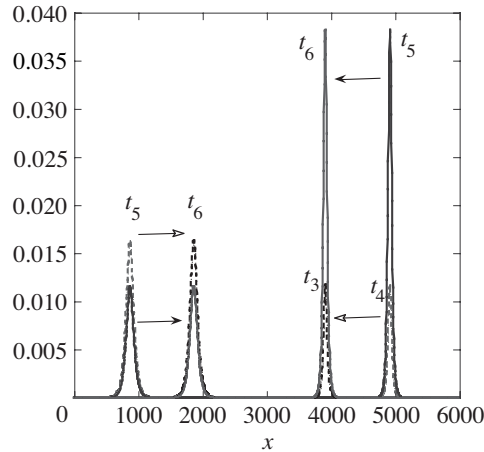


Figure 4. The detailed vector soliton solutions for modes Q_1 (dashed curves) and Q_2 (solid curves), following a second collision for the parameters given in figures 1–3 ($t_5 = 150$ K, $t_6 = 175$ K).

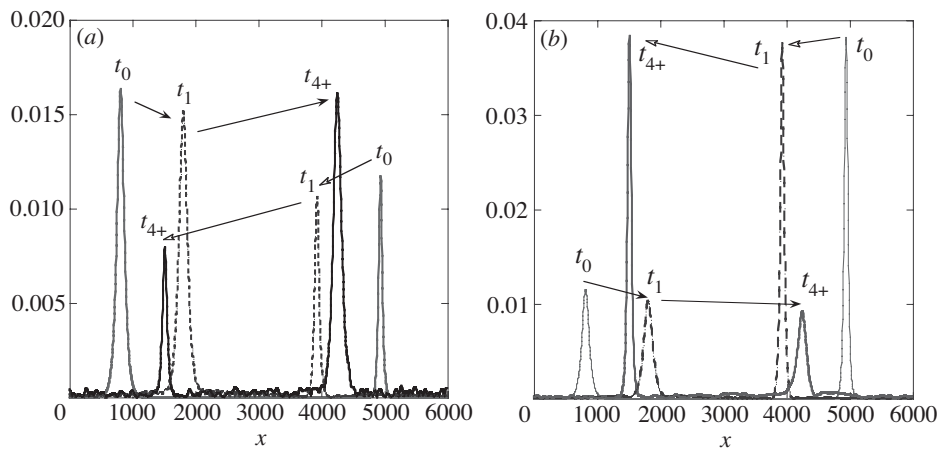


Figure 5. The propagation of the same initial pulses as in figure 1, but now down a linearly birefringent fibre in which the cross-phase modulation coefficient $B = \frac{2}{3}$. For these fibres, the coupled-NLS equations are non-integrable. The pulses no longer propagate as solitons, since their amplitudes are no longer invariant between collisions; rather, they propagate as solitary waves with the emission of small-scale radiation. Again, the total intensity in each mode $\int dx |Q_i(x, t)|^2 = \text{const.}$ is preserved to better than one part in 10^{-7} . Note that there is a left-travelling solitary wave for the mode Q_1 following the first collision ($t_{4+} = 85$ K), unlike the result for the fully integrable ($B = 1$) Manakov system.

inelastic collision for Q_1 . However, the second 1-soliton solution reappears following the second soliton–soliton collision, as shown in detail in figure 4.

(b) Coupled vector NLS of a linearly birefringent fibre

In a linearly birefringent fibre, the cross-phase modulation coefficient $B = \frac{2}{3}$ in equation (1.1), resulting in a non-integrable coupled-NLS equations. Since there is

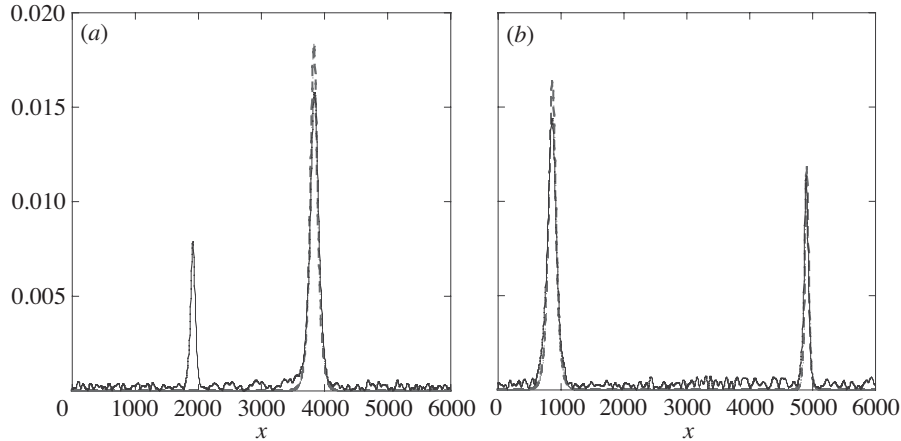


Figure 6. A detailed comparison of the pulse shapes for Q_1 following (a) the first collision, (b) the second collision for soliton solutions ($B = 1$, dashed curves) and solitary-wave solution ($B = \frac{2}{3}$, solid curves). Note the absence in (a) of the left-moving soliton for the fully integrable Manakov system ($B = 1$).

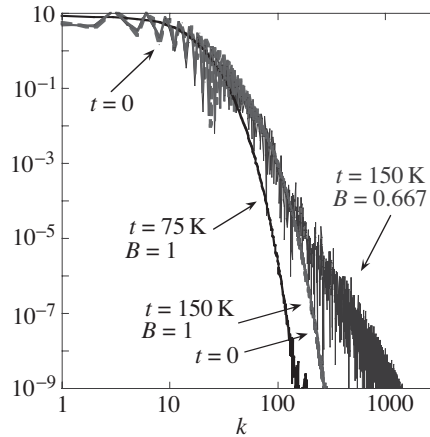


Figure 7. The intensity spectra for the Q_1 mode for both the fully integrable Manakov system ($B = 1$) at $t = 75$ K and $t = 150$ K and the mode propagation down a linearly birefringent fibre ($B = \frac{2}{3}$) at $t = 150$ K. The spectrum is narrower for the Manakov system ($B = 1$) at 75 K, since this is after the first collision and there is only one propagating soliton. Following the second collision, there are two propagating solitons and the spectrum is similar to the initial spectrum. For the linearly birefringent medium ($B = \frac{2}{3}$), the solitary waves have a similar shape to the soliton solutions (see figure 6b) but the emission of small-scale radiation gives the high- k part of the intensity spectrum.

only a slight variation in B from $B = 1$, one would expect a quasi-integrable solution. This is verified, up to a point, by our quantum lattice algorithm (figures 5 and 6). There is a slight decay in all the solitary-wave amplitudes as they propagate towards each other ($t_0 \rightarrow t_1$), with emission of radiation. In the post-collision state (t_{4+}) note that there is a quite strong solitary pulse in the Q_1 -mode that is totally absent in the fully integrable Manakov system ($B = 1$). This, and the emitted radiation for

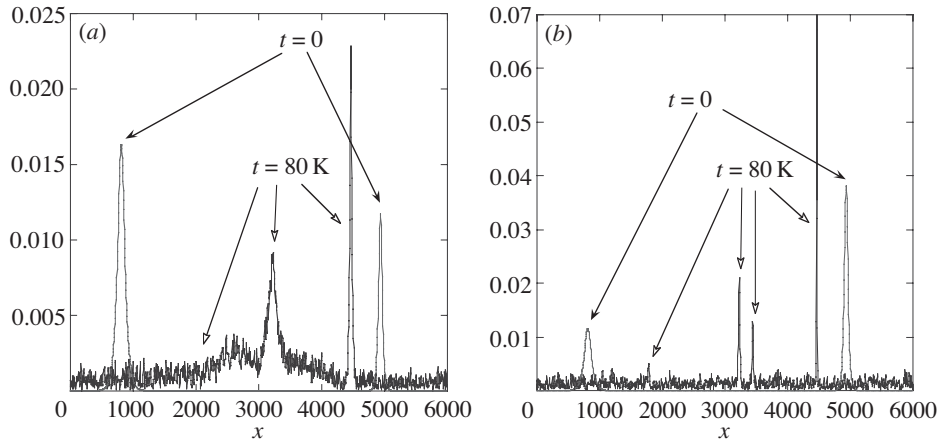


Figure 8. A coupled cubic NLS-turbulent NLS system with Q_1 integrable ($B = 1$) except for its coupling to the turbulent Q_2 -mode. The same initial conditions and parameters as in figure 1 apply. Q_1 exhibits solitary-wave behaviour, including a substantial pulse at $t = 80$ K that would be absent in a Manakov system. The background radiation is quite strong, due to the coupling to the turbulent Q_2 -mode. The Q_2 -mode exhibits δ -function-like spikes together with a short wavelength solitary-wave turbulent bath. Collisions between members of this bath, as well as with the δ -function spikes, are soliton-like. There is a locking between the spatial locations of the solitary waves in Q_1 and the location of the δ -function spikes in Q_2 .

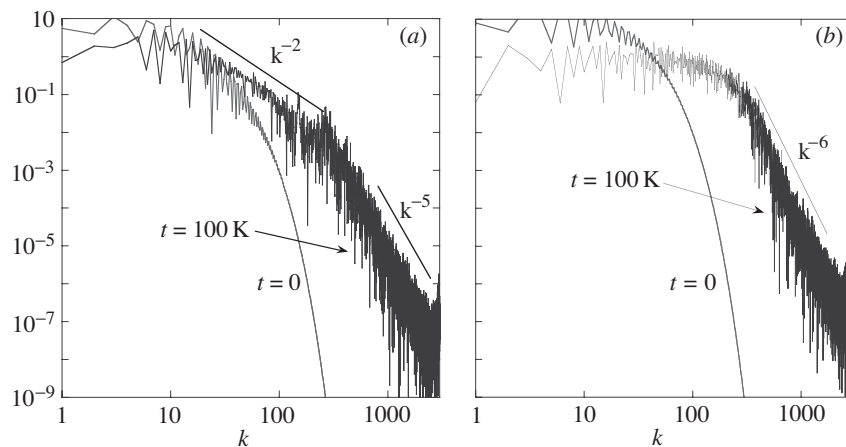


Figure 9. The intensity spectrum for the Q_1 - and Q_2 -modes for the coupled cubic NLS-turbulent NLS system. The solitary-wave structure of $|Q_1|$ results in the k^{-2} spectrum for medium scales, while the background radiation results in a k^{-5} small-scale spectrum. The turbulent $|Q_2|$ -mode exhibits white noise for medium scales and a k^{-6} small-scale spectrum.

the non-integrable case, is further highlighted in figure 6, where we compare the post-collision states of both polarization modes for $B = 1$ and $B = 0.667$.

Since it is the Q_1 mode that is the most affected by the change in the cross-phase modulation coefficient B , we examine how its intensity spectrum varies in time (figure 7). First, consider the fully integrable Manakov system, $B = 1$. As expected, the spectrum at $t = 0$ and $t = 150$ K (which is *after* the second soliton

collision and the reappearance of the second soliton in the Q_1 -mode) lie on top of each other. This is because for the fully integrable Manakov system we have simply a translation in the position of the form-invariant solitons which plays no role in the Fourier transform of $|Q_1|$. The intensity spectrum at $t = 75$ K (for $B = 1$) is significantly modified, since at this time there has only been one soliton collision and the post-collision state for $|Q_1|$ consists of only one soliton. For the linearly birefringent fibre ($B = 0.667$), we find solitary pulses and small-scale background radiation. The intensity spectrum is statistically independent of time, and the effects of the radiation emission are seen in the raised tail for wavenumbers $k > 140$. For the Q_2 -mode, the effects of variations in the cross-phase modulation coefficient B are not as pronounced with a lower level of radiation emission. As a result, we find a raised tail in the intensity spectrum for wavenumbers $k > 275$.

(c) *Quasi-turbulent soliton interactions*

We now consider the following coupled-NLS system:

$$\left. \begin{aligned} i\frac{\partial Q_1}{\partial t} + \frac{\partial^2 Q_1}{\partial x^2} + 2\mu[|Q_1|^2 + |Q_2|^2] \cdot Q_1 &= 0, \\ i\frac{\partial Q_2}{\partial t} + \frac{\partial^2 Q_2}{\partial x^2} + 2\mu\sqrt{|Q_2|^2 + |Q_1|^2} \cdot Q_2 &= 0. \end{aligned} \right\} \quad (4.1)$$

Q_1 would be governed by the integrable NLS except for its coupling to the Q_2 -mode, whose evolution is non-integrable. Again we choose the same initial profiles (equation (2.4)) and parameters as before. For the mode $|Q_1|$, the initial non-overlapping 1-solitons at $t = 0$ propagate towards each other like solitary waves with emission of radiation. By $t = 80$ K (figure 8a), the solitary waves have considerable width for this quasi-integrable mode Q_1 . The evolution of mode Q_2 is considerably different because of the underlying turbulent-evolution equation. The major peaks are extremely narrow (there are three at $t = 80$ K; see figure 8b), with the spatial locations of the two largest δ -function peaks locked to those of the two solitary waves of the Q_1 -mode. The background emission of Q_2 is also considerably different from the Q_1 -mode: it takes the form of a quasi-solitary turbulent bath of very short scales which interact with other structures such as quasi-solitons. This can be readily seen in the intensity spectra of these modes (figure 9). For the Q_1 -mode, there are two distinct spectral regions: a k^{-2} spectrum for medium range wavenumbers and a steeper, k^{-5} , spectrum for short spatial scales. The turbulent Q_2 -mode does not exhibit an intermediate spectral range, but it is flat (like white noise). For very short scales we see an intensity spectral decay of k^{-6} .

5. Conclusion

A lattice-based quantum representation is developed for the solution of coupled-NLS equations: equations that can model the propagation of pulses down a birefringent fibre. The algorithm requires two qubits per spatial node for each polarization mode and introduces quantum entanglement on the on-site qubits. This entanglement becomes strongly non-local due to the application of the streaming operator. A symmetrized form of streaming on each qubits results in a more accurate numerical

scheme (equation (3.12)), and in finite-difference form leads to an unconditionally stable algorithm. The nonlinear interaction between the polarization modes is achieved by appropriate phase transformations on all four on-site qubits, and we have tested our algorithm on a particularly exacting problem of totally inelastic vector soliton collisions of the completely integrable Manakov system.

In this vector NLS algorithm, quantum phase coherence needs to be enforced for only 16 quantum-gate operations, after which measurements are required so as to determine the amplitudes of the wave functions. These amplitudes are then used to construct the nonlinear interaction potential. It is clear that our quantum algorithm for vector solitons would be difficult to implement experimentally. Even though it is a one-dimensional model, it is complex because amplitudes must be extracted from the quantum measurement process and not simply from probabilities which are more naturally extracted from the projective von Neumann quantum measurement process over a large ensemble of molecules, as occurs in nuclear magnetic resonance spectroscopy (Pravia *et al.* 2002, 2003). Nevertheless, it is hoped that this one-dimensional quantum algorithm will serve as a stepping stone towards more complicated quantum algorithms with sufficiently many qubits per site that the experimental trade-off between the difficulty of achieving quantum entanglement and the limitation of measurable classical information that can be extracted from the quantum computer begins to work in our favour. Finally, it is interesting to note that the QLG representation is very efficiently parallelized on a classical computer.

This work was supported by the Directorate of Computational Mathematics, US Air Force Office of Scientific Research.

References

- Bialynicki-Birula, I. 1994 Weyl, Dirac and Maxwell equations on a lattice as unitary cellular automata. *Phys. Rev. D* **49**, 6920–6927.
- Frisch, U., d’Humières, D., Hasslacher, B., Lallemand, P., Pomeau, Y. & Rivet, J. P. 1987 Lattice gas hydrodynamics in two and three dimensions. *Complex Syst.* **1**, 649–676.
- Jakubowski, M. K., Steiglitz, K. & Squier, R. 1998 State transformations of colliding optical solitons and possible application to computation in bulk media. *Phys. Rev. E* **58**, 6752–6758.
- Kivshar, Y. S. & Agrawal, G. P. 2003 *Optical solitons*. Academic.
- Lakshmanan, M. & Kanna, T. 2001 Shape changing collisions of optical solitons, universal logic gates and partially coherent solitons in coupled nonlinear Schrödinger equations. *Pramana* **57**, 885–916.
- Manakov, S. V. 1974 On the theory of two-dimensional stationary self-focusing of electromagnetic waves. *JETP* **38**, 248–253.
- Menyuk, C. R. 1989 Pulse propagation in an elliptically birefringent optical Kerr medium. *IEEE J. Quantum Electron.* **25**, 2674–2682.
- Mitchell, M. & Segev, M. 1997 Self-trapping of incoherent white light. *Nature* **387**, 880–882.
- Mitchell, M., Chen, Z., Shih, M. F. & Segev, M. 1997 Self-trapping of partially spatially incoherent light. *Phys. Rev. Lett.* **77**, 490–493.
- Nielsen, M. A. & Chuang, I. L. 2000 *Quantum computation and quantum information*. Cambridge University Press.
- Peyret, R. 1996 *Handbook of computational fluid mechanics*. Academic.
- Pravia, M., Chen, Z., Yezpez, J. & Cory, D. G. 2002 Towards an NMR implementation of a quantum lattice gas algorithm. *Comput. Phys. Commun.* **146**, 339–344.

- Pravia, M., Chen, Z., Yezpez, J. & Cory, D. G. 2003 Experimental demonstration of quantum lattice gas computation. *Quant. Informat. Process.* **2**, 1–19.
- Radhakrishnan, R., Lakshmanan, M. & Hietarinta, J. 1997 Inelastic collision and switching of coupled bright solitons in optical fibers. *Phys. Rev. E* **56**, 2213–2216.
- Shor, P. W. 1994 Algorithms for quantum computation: discrete logarithms and factoring. In *Proc. 35th Annual Symp. Foundations Computer Science*. New York: IEEE Press.
- Steiglitz, K. 2001a Time-gated Manakov spatial solitons are computationally universal. *Phys. Rev. E* **63**, 016608.
- Steiglitz, K. 2001b Multistable collision cycles of Manakov spatial solitons. *Phys. Rev. E* **63**, 046607.
- Succi, S. 2001 *The lattice Boltzmann equation*. Oxford: Clarendon.
- Vahala, G., Vahala, L. & Yezpez, J. 2003a *Quantum lattice gas representation for vector solitons*. SPIE Conference Proceedings, vol. 5105, pp. 273–281. Bellingham, WA: SPIE.
- Vahala, G., Yezpez, J. & Vahala, L. 2003b Quantum lattice gas representation of some classical solitons. *Phys. Lett. A* **310**, 187–196.
- Yezpez, J. & Boghosian, B. M. 2002 An efficient and accurate quantum lattice-gas model for the many-body Schrödinger equation. *Comput. Phys. Commun.* **146**, 280–294.